Chapter 9

Monolayer and LB films of octadecanethiol and its metal complexes

9.1 Introduction

Self-assembly of organosulfur compounds on metallic surfaces like gold, silver and copper is a well known technique to obtain an ordered monomolecular film [1]. Such films provide useful systems for understanding fundamental phenomena involved at the surfaces and interfaces. The properties of the surfaces can be tailored with the choice of appropriate molecules. For instance, the surface energy can be varied continuously with the variation of the proportion of a hydrophilic terminated component in the mixed self-assembled monolayer (SAM). Self-assembled monolayer finds potential applications in the fields of wetting, dewetting, chemical sensors, biological sensors, nanolithography, molecular electronics, lubrication and optical waveguides [2–4]. Octadecanethiol ($C_{18}H_{37}SH$), an alkanethiol, is most commonly studied compound in this field. The -SH group is weakly acidic in nature and thereby the molecule becomes amphiphilic. We can expect it to form a stable monolayer at the air-water (A-W) interface. Though there are many reports on the SAM of octadecanethiol (ODT) on the metallic surfaces, there are only a few reports on Langmuir-Blodgett (LB) films of ODT molecules [5], as ODT is reported to form unstable monolayer at the A-W interface [6–9]. It is important to have a stable monolayer for the formation of defect free LB films which may find applications in devices. There were many attempts to stabilize the ODT monolayer by adding additives to the subphase. It has been

reported that the ODT monolayer can be stabilized with stearic acid provided the subphase contains barium salt [6]. Livingston and Swingley [7] have checked the stability of ODT monolayer on the aqueous subphase with different pH values and salts. They have observed that the ODT monolayer was stable only on a subphase containing potassium permanganate. Itaya *et al*. [8] have found that the ODT monolayer is stable only on the subphase containing $BaCl_2$. Bilewicz and Majda [5] have reported that the ODT monolayer can be stabilized by mixing it with octadecanol. A recent report on the surface manometry and the X-ray diffraction studies on the monolayer of ODT at the air-mercury interface have shown that ODT molecules exhibit a disordered phase of surface-parallel molecules, a condensed phase with tilted molecules and an untilted condensed phase [10].

In this chapter, we describe our studies on the ODT monolayer on ultrapure ion-free water and aqueous subphases possessing divalent and trivalent metal ions using surface manometry, Brewster angle and epifluorescence microscopy. The films were transferred on silicon substrate by LB technique and were studied using atomic force microscope.

9.2 Experimental

The compound, octadecanethiol was obtained from Aldrich. The ultrapure ion-free water having a resistivity greater than 18 MΩ-cm was used as a subphase. The subphase was made alkaline by the addition of NaOH in the ion-free water. The salts, $CdCl_2$ and $AuCl_3$.HCl were obtained from Merck. The appropriate amount of the salts were dissolved in the ion-free water and were used immediately. The solution of the ODT molecule with a concentration of 3.5 mM was prepared in HPLC grade chloroform. The compression speed of the barriers was maintained at 3.8 (Å^2/molecule)/min. The experimental details of surface manometry have been described in previous chapters. The area-relaxation curves and the equilibrium spreading pressure (ESP) of the sample were obtained as described in chapter 7. The details of Brewster angle and epifluorescence microscopy have already been described in the previous chapters. The monolayer from the aqueous subphase was transferred on solid substrates by Langmuir-Blodgett technique. The silicon (Si) wafers (one sided-polished,

0.4 mm thick) were boiled in piranha [11] solution for 10 minutes. The substrates were taken out and rinsed successively with ion-free water and ethanol. They were dried by blowing hot air at about 70 °C. The substrates were finally rinsed successively with HPLC grade chloroform and acetone. These were stored in a desiccator. Such treatments render a hydrophilic nature to the substrates. The LB films were transferred onto the treated Si substrate at a target pressure of 8 mN/m. The dipper speed was maintained at 5 mm/min. The substrate was immersed in the subphase prior to the spreading of the molecules on the subphase. The films of the ODT or its metal-complexes were transferred on the Si substrate by a single upstroke of the dipper. The atomic force microscope (AFM) imaging of the LB films were carried out using Nanoscope IIIA (Digital Instruments). All the AFM images shown here were taken in the tapping mode. Details of AFM imaging are given in chapter 5. The images were analyzed using a software, Scanning Probe Image Processor (SPIP).

9.3 Results and Discussion

9.3.1 ODT molecules at air-water and air-silicon interfaces

The surface pressure (π) − area per molecule (A_m) isotherm of ODT monolayer on the ultrapure ion-free water is shown in Figure 9.1. The isotherm shows the co-existence of gas and a condensed phase upto 19.5 Å^2. Then there is a sharp change in the slope of the isotherm indicating the onset of the condensed phase. The isotherm yields a limiting area per molecule (A_o) of 19.0 Å^2 which approximately corresponds to the cross-sectional area of the alkyl chain [12]. Hence, the steep region of the isotherm may correspond to the untilted condensed phase. The monolayer collapses at 14 mN/m followed by a plateau region.

The stability of the ODT monolayer on ion-free water at a given surface pressure was studied by monitoring the change in the normalized area, $A_t/A_{t=0}$ where A_t is the value of A_m at a time t and $A_{t=0}$ is the initial value of A_m. This is shown in Figure 9.2. Assuming a linear dependence of the normalized area with time, we get the rates of reduction of the normalized area to be 0.076 %, 0.10 % and 0.117 % per minute at the surface pressures of 2, 5 and 9 mN/m, respectively. The monolayer of the ODT molecule was quite stable as indicated

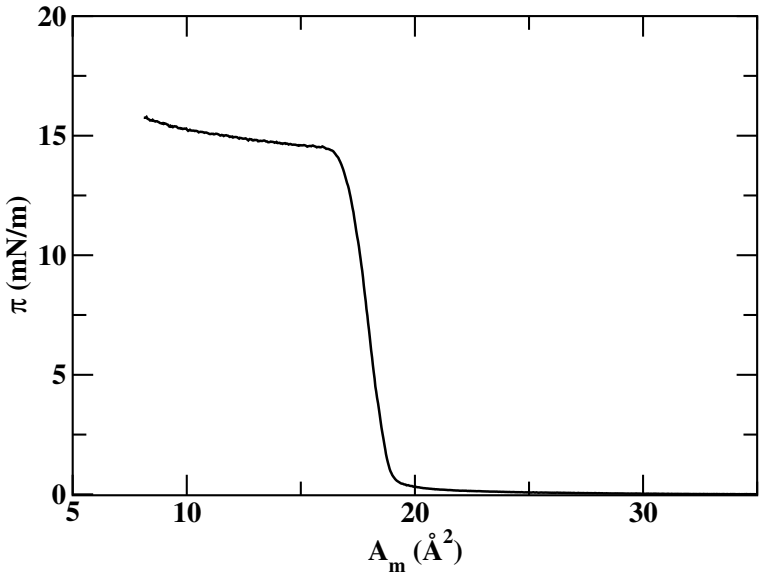

Figure 9.1: Surface pressure (π) - area per molecule (A_m) isotherm of ODT monolayer on the ultrapure ion-free water.

by the negligible rate of decrease in the normalized area. According to a model proposed

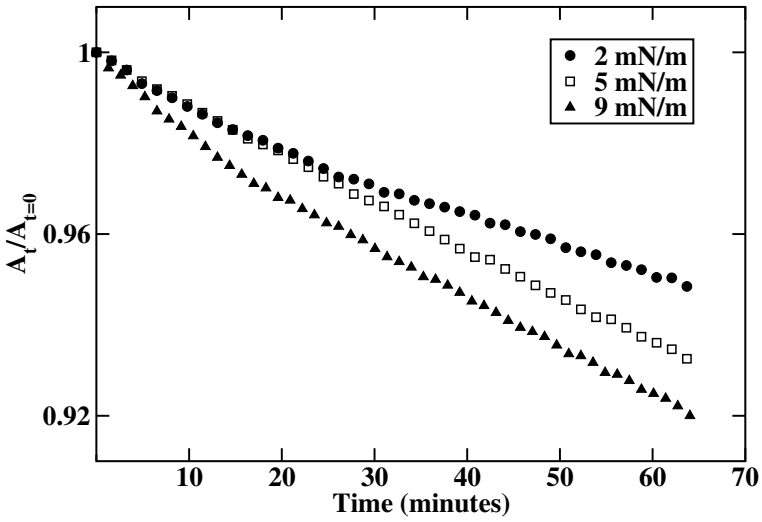

Figure 9.2: The area relaxation curves of the ODT monolayer on ion-free water at a given surface pressure. A_t is the A_m at a time t and $A_{t=0}$ is the A_m at the initial time.

by Smith and Berg [13], the decrease in normalized area can be due to the dissolution of the molecules in the subphase by diffusion, if it follows the relation $\ln(A_t/A_{t=0}) \propto -t^{\beta}$ with β equals to 0.5. However, in the present case, fitting such a power law to the data (Figure 9.2) for the surface pressures of 2, 5 and 9 mN/m yield the β values to be 0.77, 0.92 and 0.81, respectively. Hence, the small reduction in the normalized area may not be due to the

dissolution of the molecules. Such a small reduction can be attributed to the relaxation of the ODT molecules in the monolayer.

The equilibrium spreading pressure (ESP) [12] measurement of ODT molecules is shown in Figure 9.3. We find a finite ESP value (2.5 mN/m) for ODT indicating the stability of the monolayer on the ion-free water. The ESP values of the compounds like octadecanol, octadecylamine and stearic acid have been reported to be 34.3, 9 and 5.2 mN/m, respectively [13, 14]. Although these molecules are similar in structure, they differ from each other in their hydrophilic head groups. The lower value of ESP of ODT can be attributed to the less polar nature of the compound.

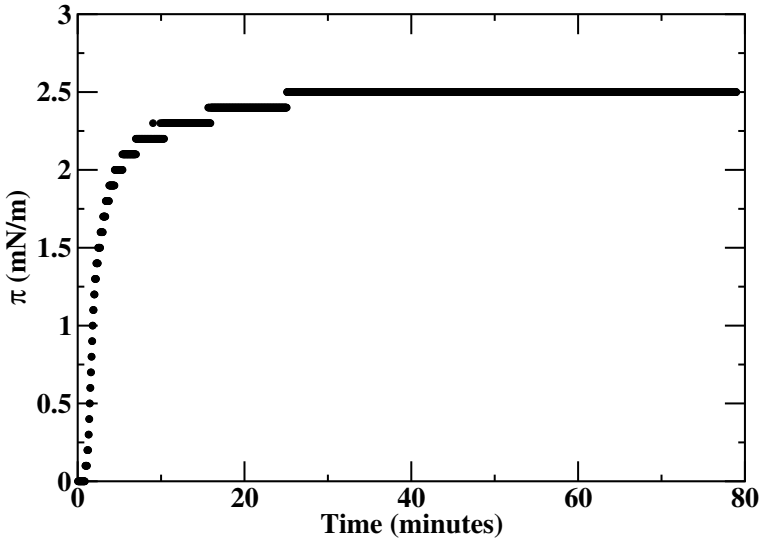

Figure 9.3: Variation of surface pressure with time for ODT molecules on ion-free water. The relative humidity and temperature were maintained at 90 % and 24 °C. The saturated value of surface pressure (2.5 mN/m) is the ESP of ODT.

The BAM images of the ODT monolayer on the ion-free water at different A_m are shown in Figure 9.4. At a large A_m, the image (Figure 9.4(a)) shows a coexistence of dark region and bright region. The dark region represents the gas phase, whereas the bright region represents the condensed phase. On compression, the bright region grows at the expense of dark region, yielding an uniform bright texture which corresponds to a homogeneous condensed phase (Figure 9.4(b)). The monolayer collapses on further compression. In the collapsed state (Figure 9.4(c)), the image shows the 3D domains (brighter region) coexisting

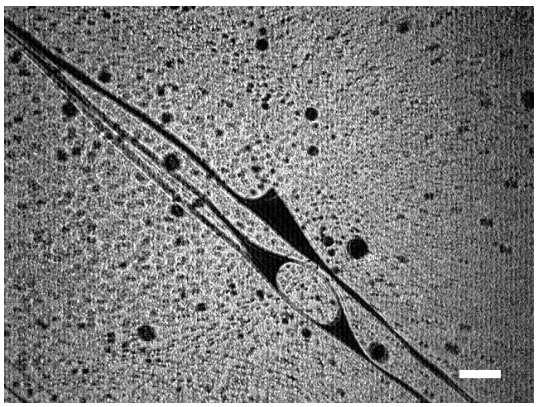

(a) A_m=30.0 Å^2

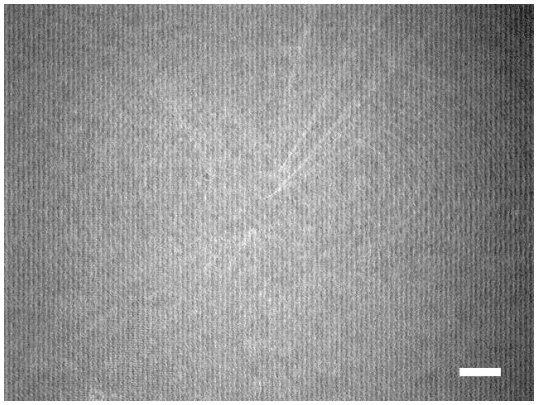

(b) A_m=18.5 Å^2

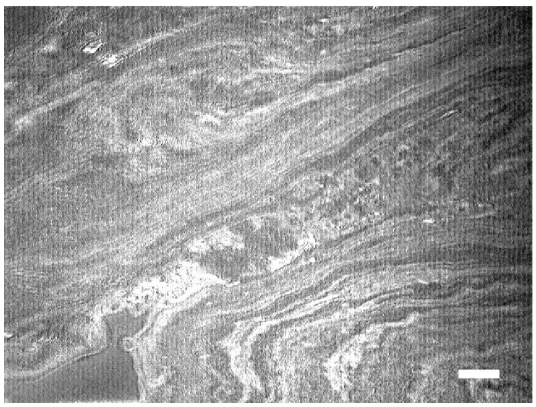

(c) A_m=15.2 Å^2

Figure 9.4: BAM images of the ODT monolayer on the ion-free water captured at different A_m. (a) shows the coexistence of gas (dark region) and condensed phase (bright region). (b) shows a homogeneous condensed phase. (c) shows the image in the collapsed state. Here, the 3D domains of ODT molecules (brighter region) are seen to coexist with the condensed phase. The scale bar represents 500 μm.

with the condensed phase (bright region).

Epifluorescence microscope images of the ODT monolayer on ion-free water are shown in Figure 9.5. The image at large A_m shows dark and the bright regions (Figure 9.5(a)). The dark region represents the gas phase. The bright region corresponds to the condensed phase of the ODT monolayer. On compression, the bright region grows at the expense of the dark region, leading to an uniform bright region, indicating a homogeneous condensed phase (Figure 9.5(b)). On further compression, the ODT monolayer collapses and the domains of different intensity levels were seen (Figure 9.5(c)). These observations were in accordance with those of the BAM imaging of the monolayer. Both microscopy techniques show an uniform texture for the condensed phase (Figures 9.4(b) and 9.5(b)) which indicates the formation of a stable ODT monolayer. An earlier study of the ODT monolayer on a water subphase of resistivity of the order of 12 MΩ-cm showed the coexistence of gas and condensed phases even in the steep region of the isotherm indicating the unstable nature of the monolayer [9]. However, we find a very stable Langmuir monolayer of ODT provided the subphase is ion-free water with at resistivity greater than 18 MΩ-cm. The phase sequence observed are; coexistence of gas and condensed phase, condensed phase and the collapsed state.

AFM studies on the LB films of ODT molecules

We have carried out AFM studies on the LB films of the ODT molecules transferred from ion-free water on hydrophilically treated silicon (Si) substrates. The reference image of the bare Si substrate for a scan range of 1×1 μm^2 is shown in Figure 9.6. The image revealed an average and a root mean square (RMS) roughnesses to be 0.122 and 0.154 nm, respectively. This shows that the Si substrates were reasonably smooth and featureless. The LB films of ODT molecules on such substrates were prepared by a single upstroke of the dipper (details are given in the experimental section). The AFM images of the LB film of ODT on Si substrate for different scan ranges are shown in Figure 9.7. The AFM images of the LB films of the ODT molecules showed some interesting results. The image for the scan range

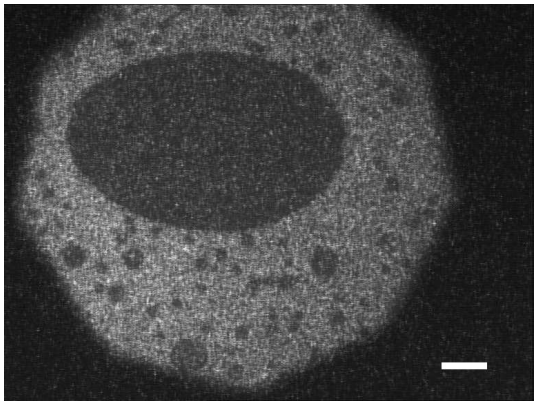

(a) A_m=30.0 Å^2

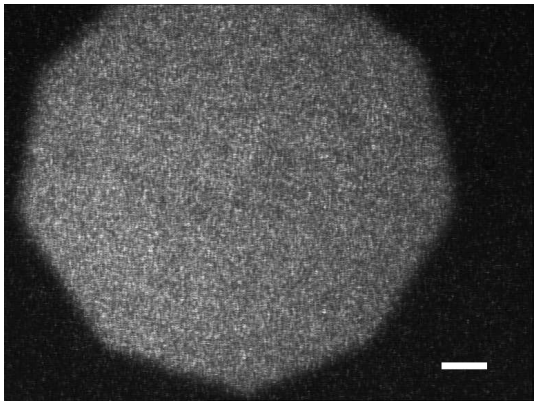

(b) A_m=18.5 Å^2

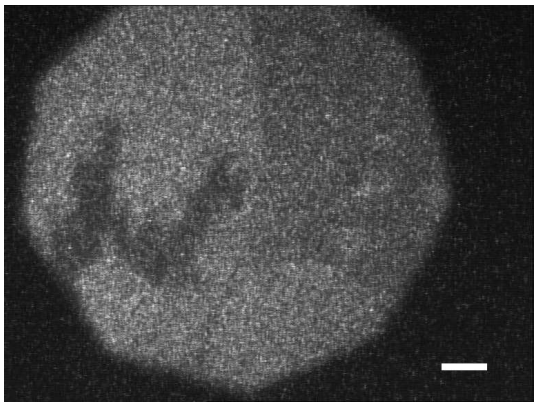

(c) A_m=15.2 Å^2

Figure 9.5: Epifluorescence images of the ODT monolayer on the ion-free water captured at different A_m. (a) shows the coexistence of gas (dark region) and condensed phases (bright region). (b) shows a homogeneous condensed phase. (c) shows the collapsed state. Here, the brighter irregular domains represent the thicker domains of the ODT molecules in the collapsed state. The scale bar represents 50 μm.

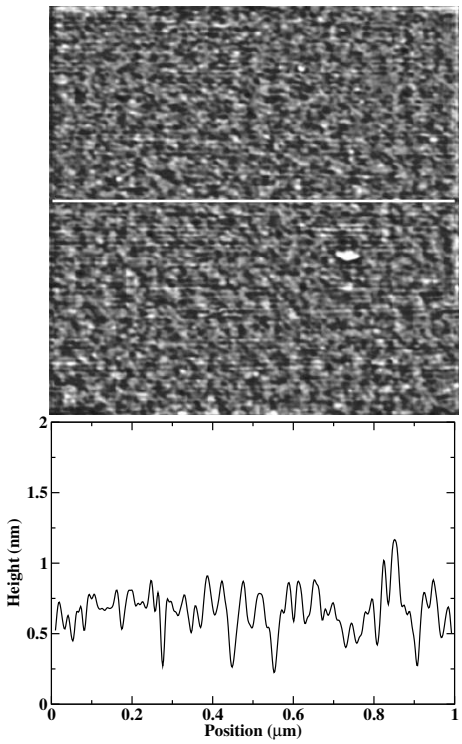

Figure 9.6: AFM image of the reference Si substrate. The white line in the image represents the line along which the height profile is drawn. The height profile is shown below the image. The size of the image is 1×1 μm^2.

of 5×5 μm^2 (Figure 9.7(a)) shows streak-like bright domains grown on the uniform gray background. Careful observation of the image reveals that there are bright and dark spots all over the gray background. The average height of the gray background is 2 nm and that of the streak domains is 4.3 nm. The image for the scan range of 1×1 μm^2 is shown in Figure 9.7(b). The image is consistent with Figure 9.7(a). Here also, the part of the streak-like domains are visible. The dark and bright spots are more prominent in this image. The uniform gray background is embedded with the bright and dark spots. The height profile along the line drawn over the image reveals the height of the bright streaks and bright spots to be around 4.2 nm. The average height of the gray background is around 2 nm. Figures 9.7(c) and 9.7(d) also show the similar features. The bright and the dark domains are more clear in Figure 9.7(c). The height profile along the line shown in the image reveals an average height of 2.3 nm for the gray background. The image also reveals bright domains, dark spots and the spots with intensity varying from gray to bright. The height profile over the bright domains

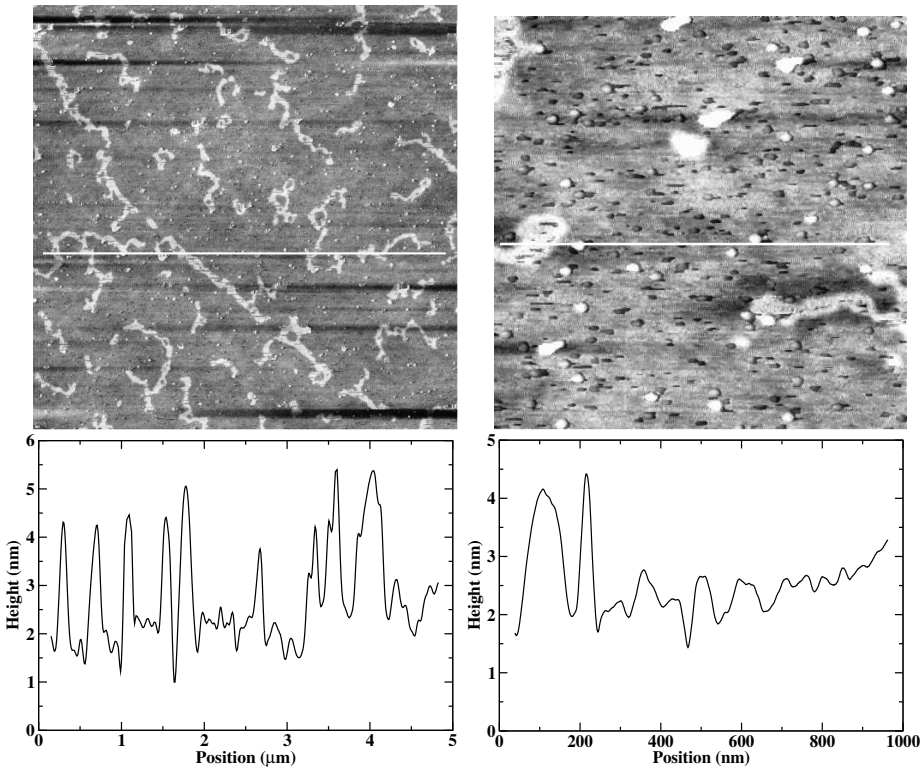

(a) 5×5 μm^2 (b) 1×1 μm^2

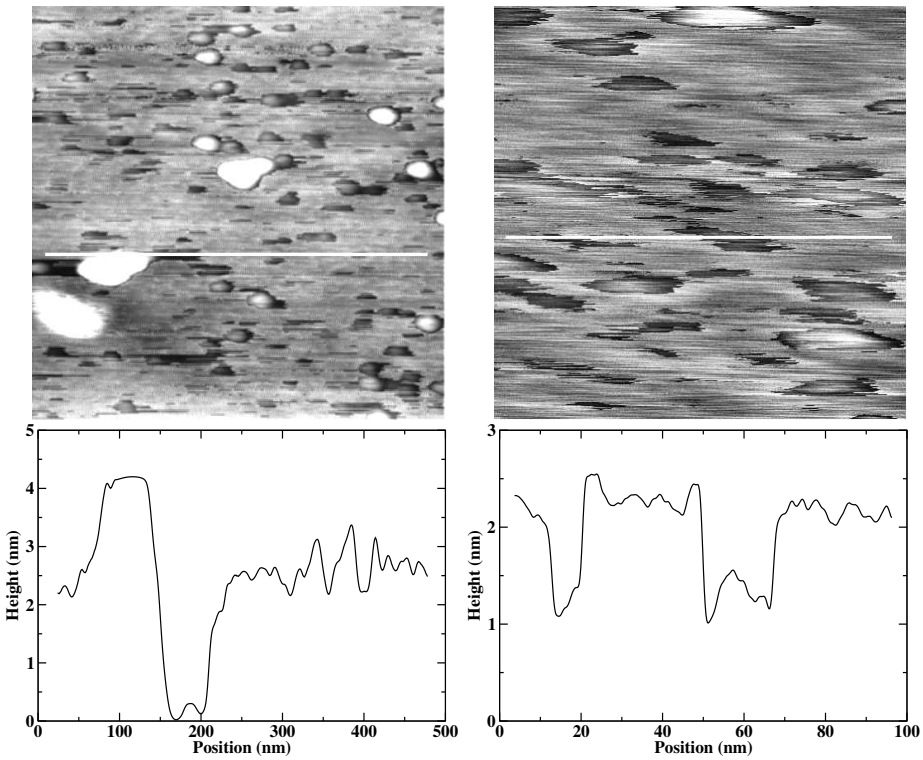

(c) 500×500 nm^2 (d) 100×100 nm^2

Figure 9.7: AFM images of the LB films of ODT for different scan ranges. The white line in the image represents the line along which the height profile is drawn. The height profiles are shown below the respective images.

yields a value of 4.2 nm. The height profile data yield the thickness of the dark spots to be nearly zero. This indicates that the dark spots are due to the bare Si substrate. The thickness of the spots with varying intensity lie in the range of 0.5 to 1.8 nm. Figure 9.7(d) shows the gray background and the domains with varying intensity. The length of the ODT molecule is 2.1 nm [15]. Hence, it can be surmised that the gray background may correspond to the monolayer of the ODT molecules where the aliphatic chains are oriented normal to the Si substrate. The streak-like domains are grown over the gray background. The average height of the streak-like domains (~4.2 nm) suggests the domains to be a bilayer of the ODT molecules oriented normal to the Si substrate. The films have defects in the form of dark domains and domains with varying intensity. The aggregation of molecules in the LB films depends highly on the nature of the substrates and the experimental parameters, such as temperature, humidity and ion contents in the subphase [16]. The molecules find a different thermodynamical environment when they get transferred from the A-W interface to the solid substrates. Hence, on the substrate the molecules relax itself in the thermodynamical stable state [17, 18]. Here, we have transferred the ODT molecules from the A-W interface in the condensed phase. In the condensed phase, the ODT molecules orient normal to the A-W interface. Through AFM imaging we could see the existence of predominantly condensed phase (gray background). However, the relaxation of the monolayer leads to the formation of streak-like bilayer domains and the defects. We sketch a schematic model, suggesting the possible arrangement of the ODT molecules in the LB film onto the Si substrates. This is shown in Figure 9.8. The gray background in the AFM images is denoted by a layer of ODT molecules oriented normal to the Si substrate. The streak-like domains are represented by the bilayer of the ODT molecules oriented normal to the substrate. The defects with varying intensity are depicted by the bunch of randomly oriented molecules and the dark spots are indicated by gaps in the film.

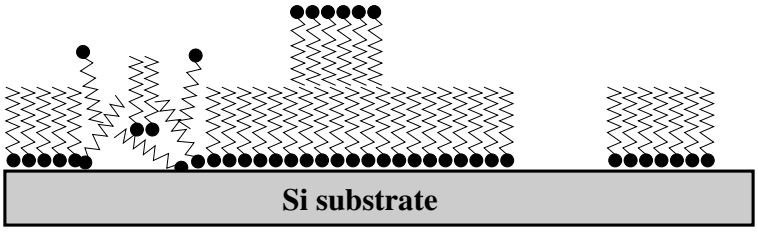

Figure 9.8: A schematic model of the arrangement of the ODT molecules in the LB film transferred from the ion-free water onto Si substrate. The -SH group is represented by black circle and the aliphatic chain is denoted by the zigzag line. Here, a layer of molecules oriented normal to the Si substrate represent the gray background in the AFM images. The streak-like domain is denoted by the bilayer of the molecules oriented normal to the substrate. The domains with intensity varying from gray to bright may represent the randomly oriented bunch of molecules (defects). The dark spots are denoted by gaps on the Si substrate.

9.3.2 Monolayer of ODT on alkaline subphase

The ODT molecule is weakly acidic in nature and hence we have studied the effect of alkaline subphase on the ODT monolayer. The effect of the presence of NaOH in the subphase on the isotherms of ODT are shown in Figure 9.9. The presence of even very small quantity

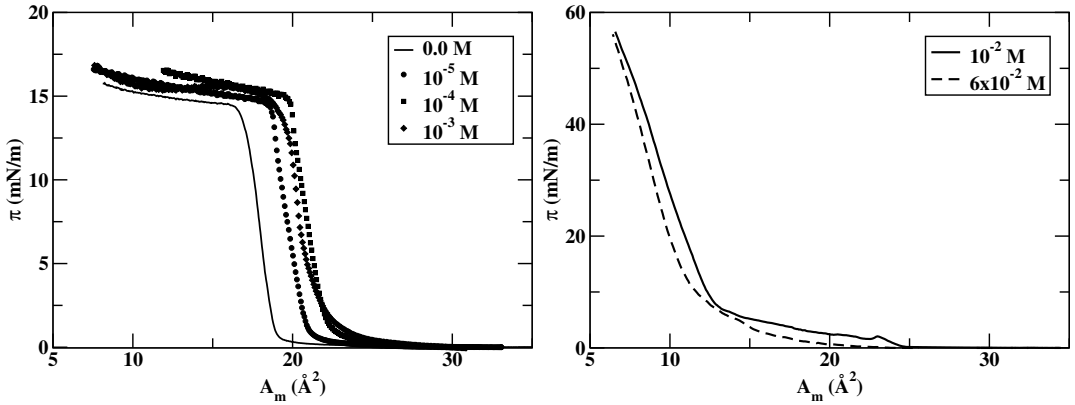

(a) (b)

Figure 9.9: Surface pressure (π) - area per molecule (A_m) isotherms of the ODT molecules with different molar concentrations of NaOH in the subphase. (a) shows the isotherms for lower NaOH concentrations ($\leq 10^{-3}$ M) in the subphase. (b) shows the isotherms for higher NaOH concentrations ($>10^{-3}$ M) in the subphase

of NaOH has a marked effect on the monolayer of the ODT molecules. The isotherms shift systematically towards higher A_m with increase in concentration ($\leq 10^{-3}$ M) of NaOH in the subphase (Figure 9.9(a)). Above the concentration of 10^{-3} M, the ODT monolayer gets

destabilized completely and the isotherms show a continuous and a gradual rise in the surface pressure (Figure 9.9(b)). The A_o values obtained from the isotherms of the ODT monolayer on the aqueous subphases containing 10^{-5}, 10^{-4} and 10^{-3} M of NaOH (Figure 9.9(a)) are 20.6, 22.1 and 22.5 $Å^2$, respectively. The acidic head group (-SH) of the ODT molecule may tend to dissociate on the alkaline subphase. The increase in A_o values may be due to the electrostatic charge repulsion between such dissociated components [12, 19]. It was further observed that holding the monolayer at a given surface pressure leads to a relatively faster decrease in A_m as compared to that of the ODT monolayer on ion-free water. This indicates an unstable nature of the monolayer on the alkaline subphase.

We have carried out the microscopy experiments on the ODT monolayer for different concentrations of NaOH in the subphase. The BAM and epifluorescence images of such monolayers are shown in Figures 9.10 and 9.11, respectively. The presence of very minute quantity of the NaOH in the subphase shows a marked change in the BAM images. In Figures 9.10(a) to 9.10(c), atleast three different phases were observed. The dark region is the gas phase, the bright region with the sharp boundary is the usual condensed phase, whereas the gray domains with diffuse boundary may correspond to the monolayer of the dissociated ODT molecules. These features were seen upto the NaOH concentration of 10^{-3} M in the subphase. Above this concentration, the crystalline flakes (brighter domains with irregular boundary) of the complex of the ODT molecules and NaOH were observed (Figure 9.10(d)). The different phases seen in the epifluorescence images were consistent with those seen in the BAM images. Here, the dark region corresponds to the gas phase, whereas the bright region represents the condensed phase. However, the diffuse region, as obtained in the BAM images, were not clearly visible in the case of epifluorescence images. The domains with irregular boundary and with different intensity levels represent the crystalline flakes of the complex of ODT molecules and NaOH (Figure 9.11(d)).

There are possibilities of the surface oxidation of the ODT molecules to form dioctadecyl disulfide over the alkaline subphase [20]. The dioctadecyl disulfide does not form a stable film over the aqueous subphase. Furthermore, the dissolution of the charged monolayer

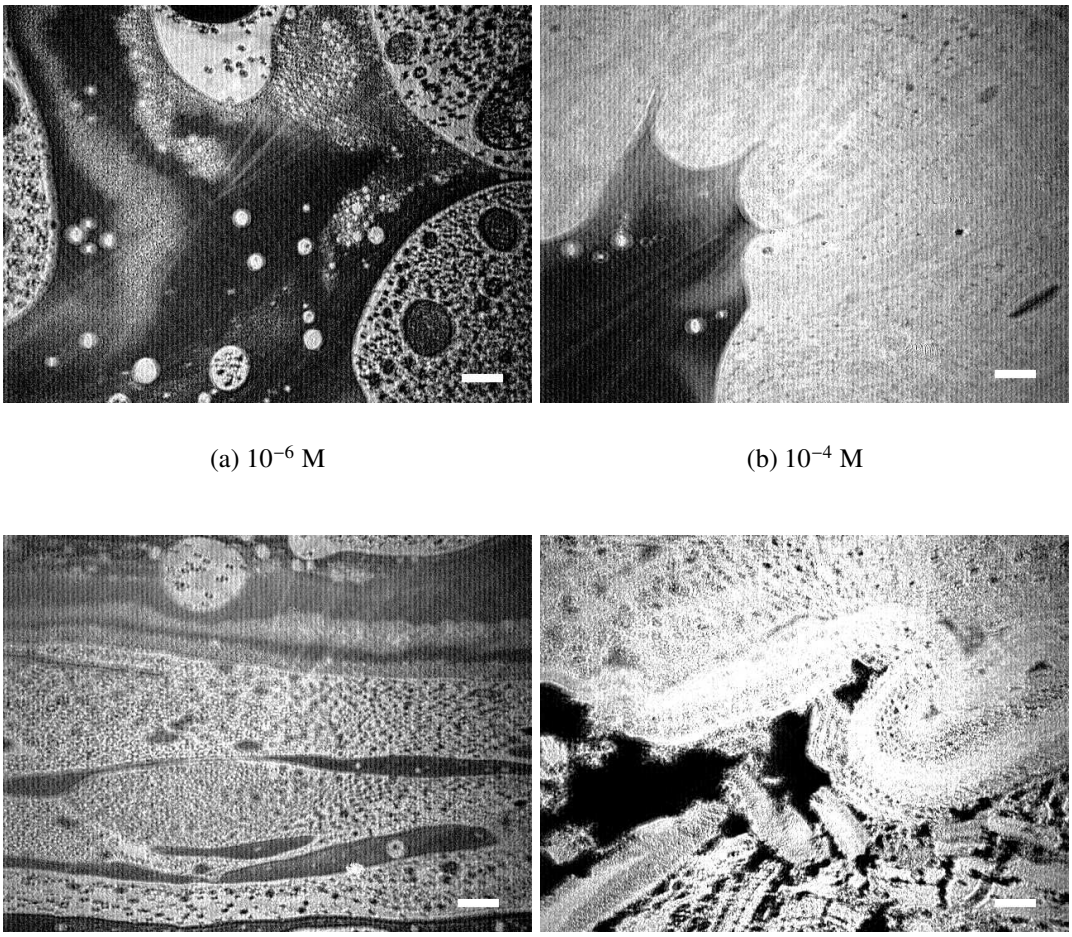

(a) 10^{-6} M (b) 10^{-4} M

(c) 10^{-3} M (d) 2×10^{-2} M

Figure 9.10: BAM images of the ODT monolayer on the aqueous subphases for various molar concentrations of the NaOH. The images have been taken for zero surface pressure and at a large A_m. In (a) to (c), the dark region represents the gas phase, the bright domains with sharp boundary represent the condensed phase and the gray domains with diffuse boundary represent the monolayer of the dissociated head groups of the ODT molecule. In (d), the brighter domains with the irregular boundary are the crystalline flakes of the complex of ODT and NaOH. The scale bar represents 500 μm.

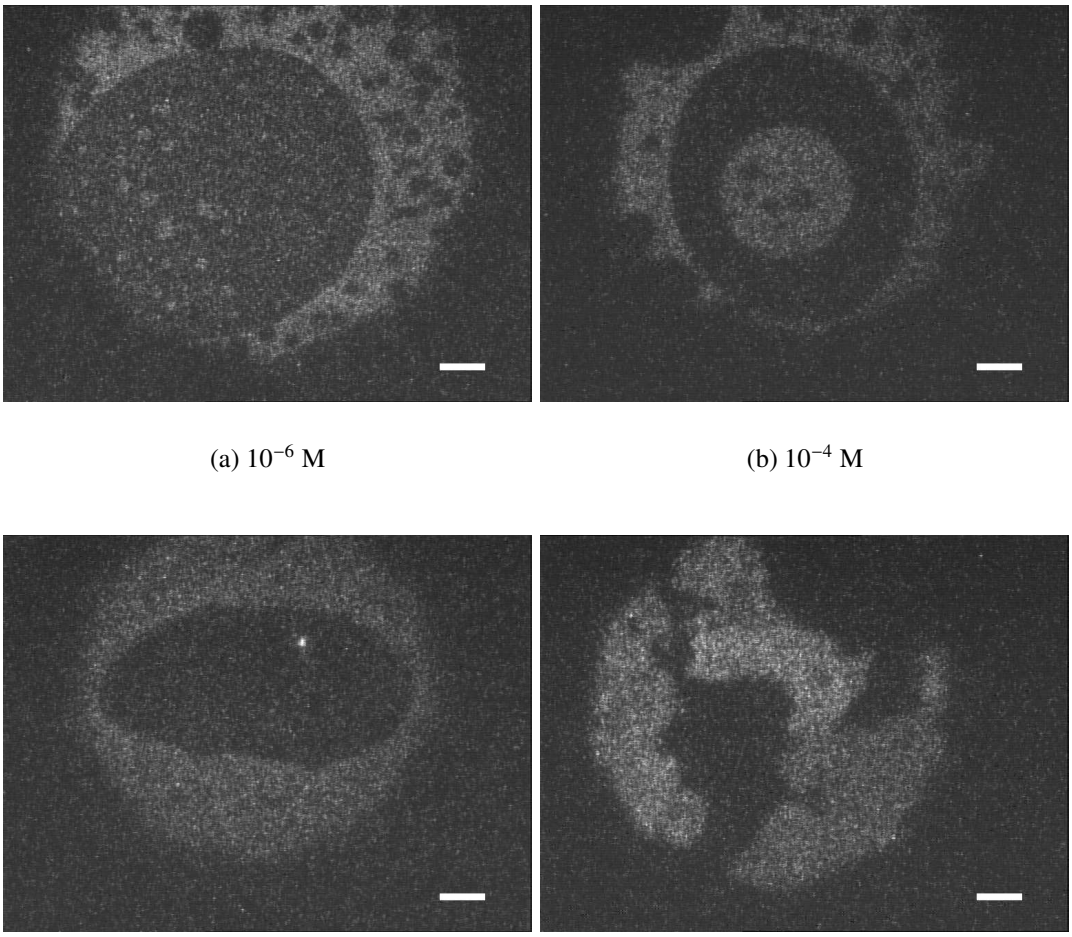

(a) 10^{-6} M (b) 10^{-4} M

(c) 10^{-3} M (d) 2×10^{-2} M

Figure 9.11: Epifluorescence images of the ODT monolayer on the aqueous subphases for various molar concentrations of the NaOH. The images have been taken for zero surface pressure and at a large A_m. In (a) to (c), the dark, bright and the diffuse region represent the gas phase, condensed phase and the monolayer with the dissociated head groups, respectively. The contrast in the images are poor due the quenching of dye in the alkaline medium. In (d), the domains with irregular boundary and different intensity levels represent crystalline flakes of complex of ODT and NaOH. The scale bar represents 50 μm.

is more as compared to the uncharged monolayer [12]. Hence the instability of the ODT monolayer on the alkaline subphase can be attributed to the dissociation of the ODT head group and the formation of the disulfide during the surface chemical oxidation.

9.3.3 Metal complexes of ODT molecules

9.3.3.1 Effect of divalent ions (Cd^{2+}) in the subphase

We have studied the effect of divalent ion (Cd^{2+}) in the subphase on the films of the ODT molecules at the A-W interface and on air-solid interface. It is known that a Cd^{2+} ion makes complex with two ODT molecules in order to achieve electroneutrality. In the complex unit, it has been proposed that the orientation of the aliphatic chain of the two ODT molecules are in opposite direction with the Cd^{2+} ion at the center [8]. Therefore, the formation of complex at the A-W interface may reduce the area per molecule.

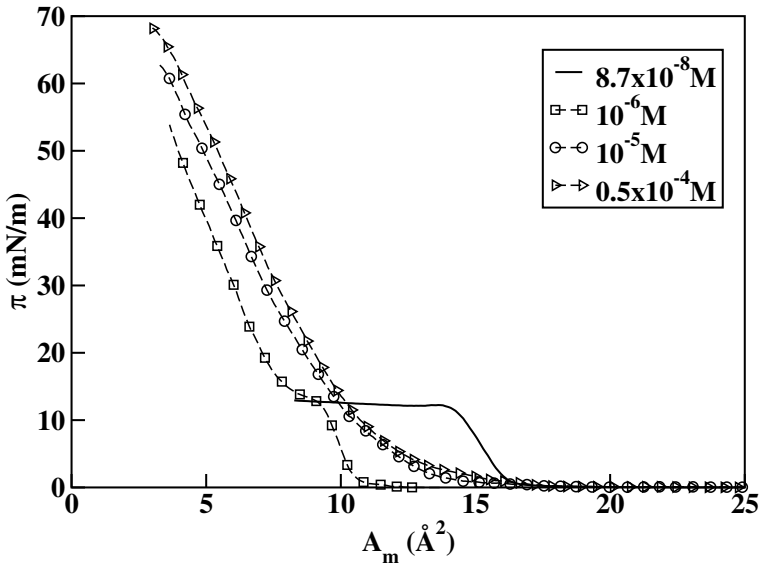

Figure 9.12: The surface pressure (π) - area per molecule (A_m) isotherms of the ODT monolayer for different molar concentrations of $CdCl_2$ in the aqueous subphase.

The isotherms of the ODT molecules on the aqueous subphases having different molar concentrations of $CdCl_2$ are shown in Figure 9.12. We find a drastic change in the π-A_m isotherm of the ODT due to the presence of small amount of $CdCl_2$ in the aqueous subphase. For a very low concentration (8.7×10^{-8} M) of $CdCl_2$ in the aqueous subphase, the trend of the isotherm was similar to the one obtained for the ion-free water. However, there is a shift

in the limiting area per molecule (A_o). It shows the value of A_o to be 16.5 Å^2. The isotherm for the concentration of 10^{-6} M shows similar trend but the surface pressure continues to increase after an initial collapse at around 13 mN/m. It shows the A_o value to be 10.5 Å^2. The isotherms for higher concentrations show a different behavior. They show a gradual rise in the surface pressure to very large values ($\geq$ 60 mN/m). The trend of the isotherms do not change on further increase in the concentration of $CdCl_2$. Here, the values of A_o lie in the range of 10.5 to 11.5 Å^2. These values are about half of those corresponding to the normally oriented molecules in the condensed phase of ODT at the A-W interface. This indicates the formation of bilayer of the complex of ODT and $CdCl_2$ [8]. The A_o value (= 16.5 Å^2) for the lower concentration (8.7×10^{-8} M) is more than for a bilayer. This can be suggested as the formation of the complex of the ODT molecules in a fraction of the monolayer with $CdCl_2$. The BAM and the epifluorescence images of the ODT monolayer for an aqueous subphase containing 8.7×10^{-8} M of $CdCl_2$ are shown in Figure 9.13. In the BAM image

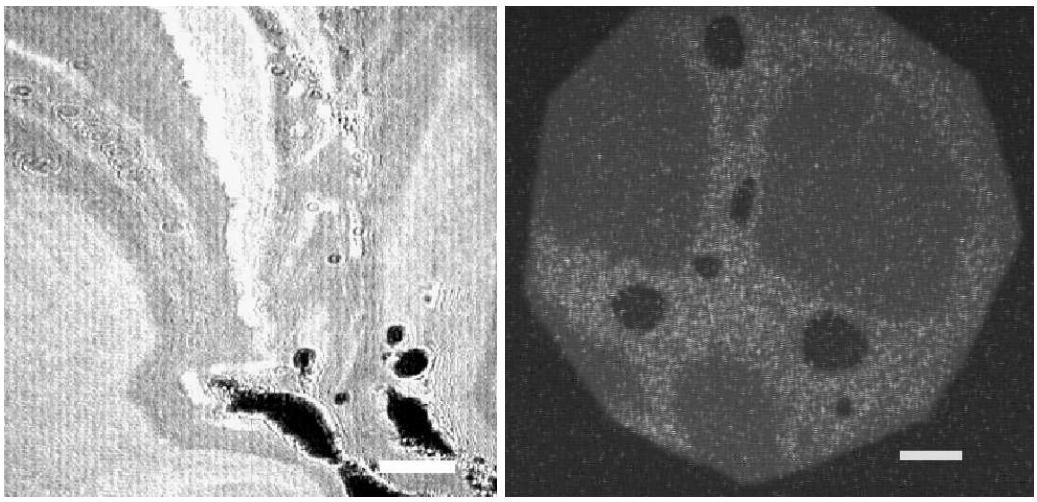

(a) A_m=27.5 Å^2 (b) A_m=27.5 Å^2

Figure 9.13: (a) and (b) represent the BAM and the epifluorescence images of the ODT monolayer on an aqueous subphase containing 8.7×10^{-8} M of $CdCl_2$, respectively. The images were captured at a large A_m and zero surface pressure. In (a), the dark domains represent the gas phase. The gray region in the background represents the condensed phase of the ODT molecules and the bright region represents domains of the complex of ODT and $CdCl_2$. In (b), the dark region represents the gas phase, the gray region represents the domains of the complex of ODT and $CdCl_2$ and the bright region represents condensed phase of the ODT molecules. The scale bars in (a) and (b) represent 500 and 50 μm, respectively.

(Figure 9.13(a)), there are dark domains and gray domains with the different intensity levels. The dark region represents the gas phase. The gray region may represent the condensed phase of the ODT molecules. The bright domains may represent the bilayer of the complex of ODT and $CdCl_2$. In the epifluorescence image (Figure 9.13(b)), the dark domains represent the gas phase and the bright background represents the condensed phase of the ODT molecules. The gray and irregular domains may represent the bilayer of the complex of ODT and $CdCl_2$. The domains of the complex are darker than that of the condensed phase of the ODT molecules due to a poor miscibility of dye molecules in it.

AFM studies on the LB films of ODT-$CdCl_2$ complex

The effect of $CdCl_2$ in the subphase on the LB films of the ODT molecules was studied using AFM. The films of the complex of ODT molecules with $CdCl_2$ were transfered on hydrophilic Si substrates by LB technique as discussed in the experimental section. The AFM images of the films for the two different scan ranges are shown in Figure 9.14. Figure 9.14(a) shows a dendrite-like structure over an uniform background. The height variation data reveal that the uniform background has an average height of 2 nm. The average thickness of the dendrite-like structure above the uniform gray background is 4.5 nm. An image with a lower scan range is shown in Figure 9.14(b). This image also shows an uniform background of thickness of about 2 nm and the average thickness of the dendrite-like domain to be 4.4 nm. The height variation in the dendrite-like domains is very small suggesting the uniform thickness of the dendritic domains. The features in both the images scale according to the scan range indicating its reproducibility. The length of the ODT molecule is 2.1 nm, and the length of the complex unit for all trans conformation of the aliphatic chain is around 4.5 nm. [15]. According to the model proposed by Itaya *et al*. [8], the complex unit represent a bilayer of the complex of ODT molecules with Cd^{2+} ion. Therefore, we can propose that the uniform background represents an ODT monolayer on Si substrate with the molecules being oriented normal to the substrate. The height variations obtained from the Figure 9.14 indicate that the dendrite-like domains may correspond to that of a layer of the complex unit

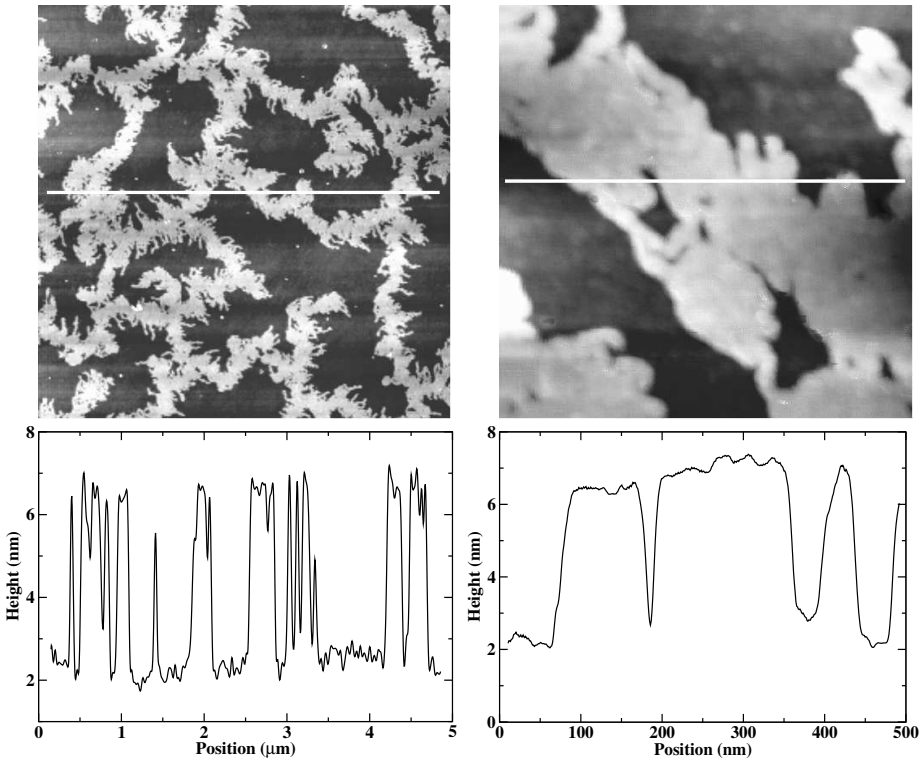

(a) 5×5 μm^2 (b) 500×500 nm^2

Figure 9.14: AFM images of the LB films of ODT molecules deposited from an aqueous subphase containing 8.7×10^{-8} M of $CdCl_2$. The white line in the image represents the line along which the height profile is drawn. The height profiles are shown below the respective images.

of ODT and $CdCl_2$. The complex unit behaves like a hydrophobic component that cannot anchor to the water surface. We suggest that the monolayer at the background are composed of ODT molecules and the layer complex unit is deposited on it. Based on our experimental observations, we present a schematic diagram showing a model for the aggregation and arrangement of the ODT molecules in the LB film at the air-silicon interface. This is shown in Figure 9.15. In the model, it is shown that the first monolayer is composed of ODT

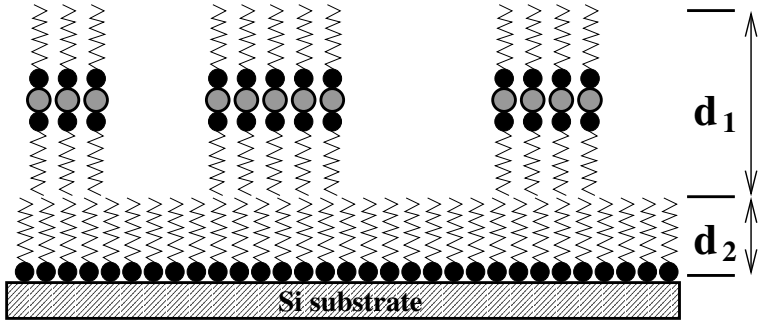

Figure 9.15: A schematic model of the arrangement of the molecules in the LB films deposited from the subphase containing 8.7×10^{-8} M of $CdCl_2$. The polar group of the ODT molecule is represented by the black circle and the chain is represented by the zigzag lines. The Cd^{2+} ion is represented by gray circle. d_1 and d_2 represent the thicknesses of the monolayer of the normally oriented ODT molecules (gray background in the AFM images) and a layer of the complex unit (dendrite-like domains in AFM images), respectively. The experimentally obtained average values of d_1 and d_2 are 2.0 and 4.5 nm, respectively.

molecules where all the molecules are normally oriented on the Si substrate. In the layer of the complex unit, which forms a dendrite-like structure in the AFM images, the two ODT molecules face each other with the Cd^{2+} at the center. The AFM images suggest the values for the thickness d_1 and d_2 (as shown) to be 2 and 4.5 nm, respectively.

9.3.3.2 Effect of trivalent ions (Au^{3+}) in the subphase

We have studied the effect of trivalent ion (Au^{3+}) in the aqueous subphase on the films of ODT molecules at the A-W interface and the air-solid interface. It is possible that a Au^{3+} ion forms complex with three ODT molecules in order to achieve electroneutrality. The isotherms for the different molar concentrations of $AuCl_3$.HCl in the aqueous subphase are shown in Figure 9.16. For the lower concentrations of $AuCl_3$.HCl (3.15×10^{-7} and 10^{-6} M) in the subphase, the trend of the isotherms are similar to those for ion-free water. However,

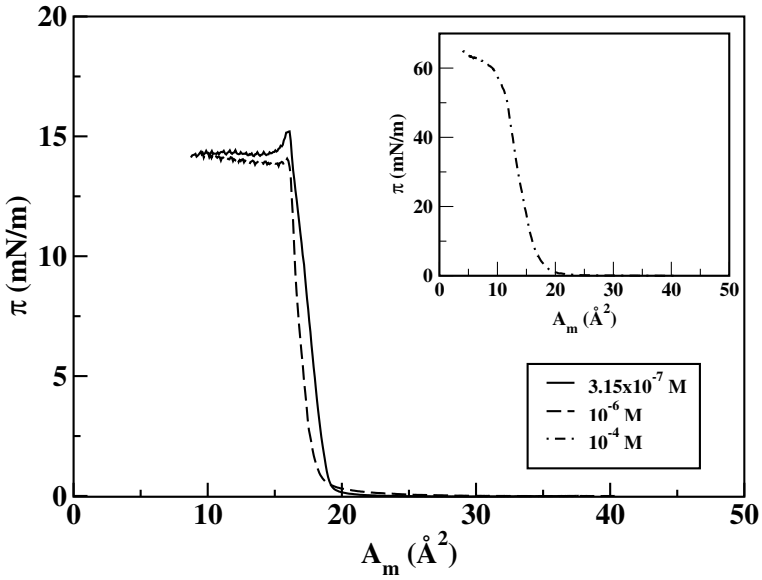

Figure 9.16: Surface pressure (π) - area per molecule (A_m) isotherms of ODT monolayer for different molar concentrations of $AuCl_3$.HCl in the aqueous subphase. For visual clarity, the isotherm for 10^{-4} M is shown in the inset. Here, the surface pressure increases to a very high value of 60 mN/m.

there is a slight shift in the A_o to the lower values. For the higher concentration (10^{-4} M), the isotherm showed a gradual rise in surface pressure to a very high value ($\sim$ 60 mN/m). However, there is no significant change in the A_o value. The values of A_o obtained from the isotherms for the $AuCl_3$.HCl concentrations of 3.15×10^{-7}, 10^{-6} and 10^{-4} M in the subphase were 19.0, 18.0 and 17.0 Å^2, respectively. These numbers suggest that the complex unit of ODT and Au^{3+} may orient normal to the water surface. The small shift in the isotherm can be attributed to the condensation of the monolayer by the trivalent Au^{3+} ion. The condensation of fatty acid monolayer with trivalent ion (Al^{3+}) has been reported in literature [21].

The BAM images for the two different concentrations of $AuCl_3$.HCl in the aqueous subphase are shown in Figure 9.17. The BAM image for a concentration of 3.15×10^{-7} M of $AuCl_3$.HCl shows an uniform texture in the steep region of the isotherm (Figure 9.17(a)). This is similar to the condensed phase of the ODT monolayer on the ion-free water (Figure 9.4(b)). At this concentration, the circular and mobile domains were seen at a large A_m. This indicates a fluidic nature of the monolayer. The BAM images for a concentration of 10^{-4} M of $AuCl_3$.HCl are shown in Figure 9.17(b). The compression of the monolayer yields an uniform gray texture (Figure 9.17(b))(A). During expansion, the film shows cracks

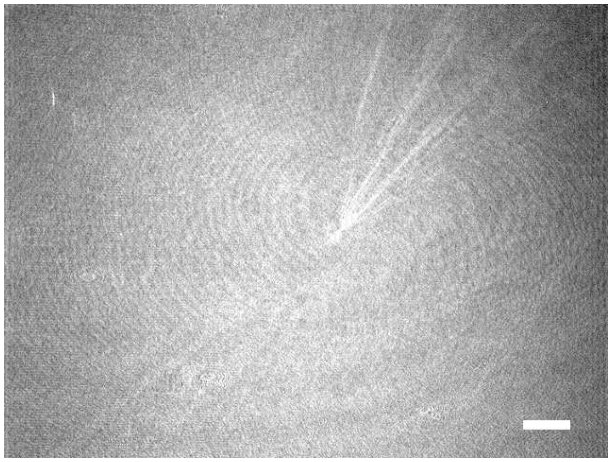

(a) 3.15×10^{-7} M

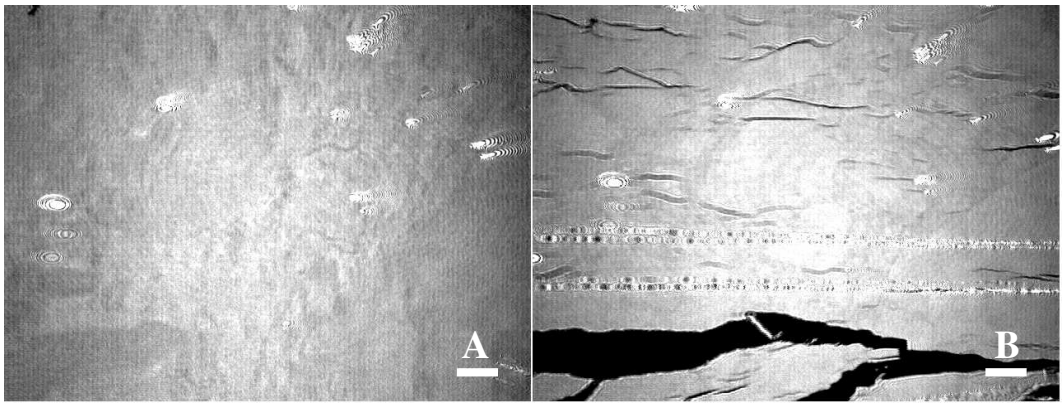

(b) 10^{-4} M

Figure 9.17: BAM images of the ODT monolayer on the aqueous subphase for different molar concentrations of $AuCl_3$.HCl. The concentration of the salt in the subphase is given below the respective images. The images were captured at A_m of 19.0 Å^2. (a) shows a very uniform gray texture. In (b), **A** represents the monolayer during compression of the film, whereas **B** represents during expansion at the same A_m. **A** shows an uniform gray texture. **B** shows dark domains (gas phase) and gray domains with sharp boundaries.

with sharp boundaries (Figure 9.17(b))(B). This indicates a crystalline nature of the film.

AFM studies on the LB films of ODT-$AuCl_3$.HCl complex

The effect of $AuCl_3$.HCl in the aqueous subphase on the LB films of ODT molecules was studied using AFM. The preparation of LB films of ODT with $AuCl_3$.HCl in the aqueous subphase is described in the experimental section. Figure 9.18 shows the AFM image of the

LB film of the complex of ODT and $AuCl_3$.HCl. It reveals the domains with predominantly

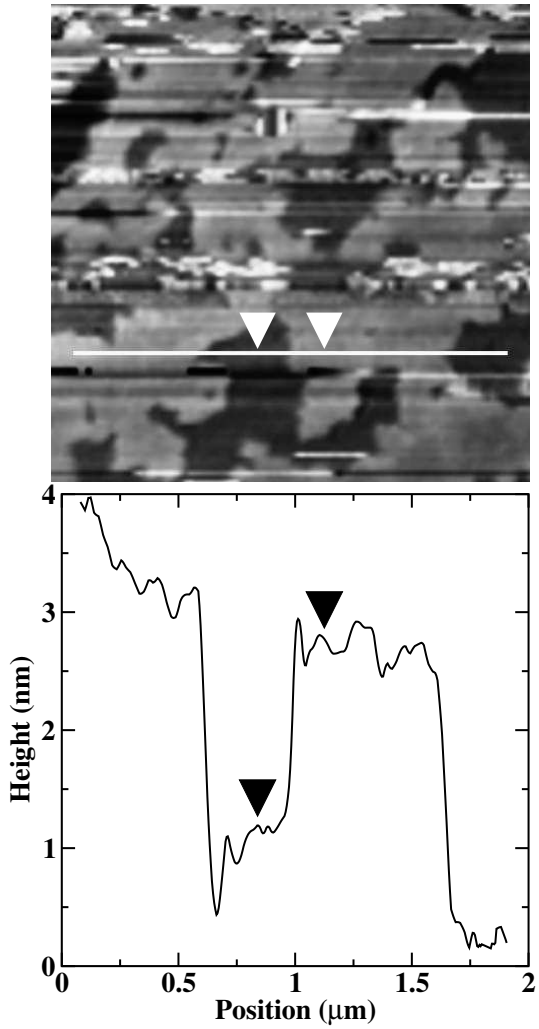

Figure 9.18: AFM image of the LB film of ODT molecules deposited from an aqueous subphase containing 3.15×10^{-7} M of $AuCl_3$.HCl. The white line in the image represents the line along which the height profile is drawn. The height profile is shown below the image. The arrows in the height profile plot are shown to depict the points which yield a height difference to be around 2 nm. The size of the image is 2×2 μm^2.

two different thicknesses (dark and gray regions). The thickness of the dark region was found to be very small. Hence, this region may correspond to the bare Si substrate. The height profile data indicate that the average thickness of the gray domains is around 2 nm. Therefore, the gray region may correspond to the domains of the ODT molecules oriented normal to the substrate. Some thick domains (bright region) are also seen in the image which may correspond to the domains of the complex of ODT and $AuCl_3$.HCl.

9.4 Conclusions

We have performed a systematic study on the Langmuir monolayer and the Langmuir-Blodgett films of ODT and ODT-metal complexes. We have shown that the ODT monolayer is stable at the A-W interface provided the water is ion-free having a resistivity greater than 18 MΩ-cm. However, the monolayer is very sensitive to the presence of very small quantities of NaOH or the salts ($CdCl_2$ and $AuCl_3$.HCl) in the aqueous subphase. The possibility of the surface oxidation of the ODT molecule may also play role in destabilizing the monolayer. The ODT molecules predominantly prefer an orientation normal to the Si substrate, as observed using the AFM. Interestingly, the AFM images reveal streak-like domains which are the bilayer of the ODT molecules. The ODT monolayer behaves differently with divalent and trivalent ions in the subphase. The presence of divalent ion (Cd^{2+}) in the subphase reveals the formation bilayer at the A-W interface. The AFM images of the LB film of the ODT molecules deposited from an aqueous subphase containing the very low concentration of $CdCl_2$ reveal the dendritic domains. The dendritic domains represent a layer of the complex unit. A crystalline monolayer was observed due to the presence of trivalent ions. The BAM images showed an uniform crystalline films. The AFM images of the LB film of ODT molecules deposited from a subphase containing very low concentration of $AuCl_3$.HCl show the domains of ODT molecules oriented normal to the substrate and thick domains of the complex of ODT and $AuCl_3$.HCl.

The stable Langmuir monolayer of the ODT molecules can be transferred onto substrates by LB technique which may have potential applications in device fabrication. ODT molecules can be used as an adhesion promoter for the transfer of LB films of poorly adsorbing compounds. We have demonstrated the formation of LB films of ODT on Si substrate. The streak-like domains can be employed for the growth of nanowires.

Bibliography

[1] A. Ulman, Chem. Rev. **96**, 1533 (1996).

[2] I. Rubinstein, S. Steinberg, Y. Tor, A. Shanzer, and J. Sagiv, Nature (London) **332**, 426 (1988).

[3] C. J. Zhong and M. D. Porter, Anal. Chem. **67**, 709A (1995).

[4] G. M. Whitesides and P. E. Laibinis, Langmuir **6**, 87 (1990).

[5] R. Bilewicz and M. Majda, Langmuir **7**, 2794 (1991).

[6] H. Sobotka, S. Rosenberg, in H. Sobotka (Ed.), Monomolecular Layers., Amer. Ass. Advan. Sci., Washington DC, 1954, p 175.

[7] H. K. Livingstone and C. S. Swingley, J. Colloid Interface Sci. **38**, 643 (1972).

[8] A. Itaya, M. Van der Auweraer, and F. C. De Schryver, Langmuir **5**, 1123 (1989).

[9] W. Zhao, M. W. Kim, D. B Wurm, S. T. Brittain, and Y. T. Kim, Langmuir **12**, 386 (1996).

[10] B. M. Ocko, H. Kraack, P. S. Pershan, E. Sloutskin, L. Tamam, and M. Deutsch, Phys. Rev. Lett. **94**, 017802 (2005).

[11] Piranha solution is a mixture of conc.H_2SO_4 and H_2O_2 in ratio of 3:1 (by volume). The solution is very dangerous and it has to be handled carefully.

[12] G. L. Gaines, Jr., *Insoluble Monolayers at Liquid-Gas Interfaces* (Wiley-Interscience, New York, 1966).

[13] R. D. Smith and J. C. Berg, J. Colloid Interface Sci. **74**, 273 (1980).

[14] Y. L. Lee and K. L. Liu, Langmuir **20**, 3180 (2004).

[15] ACD/ChemSketch, Freeware Version 5.12, Advanced Chemistry Development, Inc., Toronto ON, Canada, www.acdlabs.com, 2002.

[16] J. A. Zasadzinski, R. Viswanathan, L. Madsen, J. Garnaes, and D. K. Schwartz, Science **263**, 1726 (1994).

[17] H.D. Sikes, J.T. Woodward, and D.K. Schwartz, J. Phys. Chem. **100**, 9093 (1996).

[18] H.D. Sikes and D.K. Schwartz, Langmuir **13**, 4704 (1997).

[19] M. Yazdanian and H. Yu, G. Zografi, Langmuir **6**, 1093 (1990).

[20] J. Ahmad, Langmuir **12**, 963 (1996).

[21] G. Roberts, *Langmuir-Blodgett Films* (Plenum, New York, 1990).

Appendix A

Functionalized gold particles

The functionalized gold particle (FGP) was synthesized by Prof. Sandeep Kumar of our Institute. These particles typically have an average core size of 5.5 nm and they belong to the class of nanoparticles. Hexanethiolate-stabilized gold particles were prepared using a method described by Song *et al*. [J. Am. Chem. Soc. **125** 11694 (2003)]. A solution of tetraoctylammonium bromide (1.1 g) in toluene (65 ml) was added to a solution of 158 mg of $HAuCl_4$.3H2O. The solution was stirred for 20 minutes, and then n-hexanethiol (142 mg) was added with further stirring for 10 minutes. At this stage, a solution of 450 mg of $NaBH_4$ in 5 ml of water was added. The reaction mixture was stirred at room temperature for 24 hours. The organic phase was separated, evaporated to about 2-3 ml in a rotary evaporator under vacuum at room temperature, mixed with 50 ml ethanol and centrifuged at 5000 rpm for 1 hour. The supernatant was removed. The resulting hexanethiol-protected gold particles were dissolved in about 1 ml of dichloromethane and precipitated with ethanol. The centrifugation and redispersal process was repeated several times to ensure the complete removal of non-covalently bound organic material. Removal of the solvent afforded 60 mg of hexanethiol-caped gold particles. To prepare mixed monolayer protected gold particles, a solution of above particles (12 mg) in about 1 ml of dichloromethane and 4 mg of 11-mercapto-1-undecanol in about 1 ml of THF was stirred for 48 hours. The purification was performed as described above. ^{1}H NMR analysis of the product indicates the presence of mercapto-1-undecanol and hexanethiol moieties in 2:1 ratio. The functionalized gold particles obtained by the above method were amphiphilic in nature.

Appendix B

Instrumentation for reflection absorption infrared spectroscopy: Study of tilt and ordering of the molecules in the LB films

We have designed and fabricated an accessory to an FTIR spectrometer to study the molecular tilt and ordering in the Langmuir-Blodgett (LB) films by employing the technique of grazing angle reflection absorption infrared spectroscopy (RAIRS). We have simulated numerically an IR spectrum of an isotropic film of monomolecular thickness. Such a spectrum was utilized to determine the tilt of the molecules in the LB film deposited on a substrate. The variable-temperature RAIRS was used to detect an order-disorder phase transition of the LB films of stearic acid.

Instrumentation for RAIRS

The schematic diagram of a wedge-setup employed for the RAIRS is shown in Figure B.1. A brass block (W) having a dimension of 7.5x2.5x6.5 cm^3 was machined to obtained a wedge shaped structure. The wedge angle (α) was made 176° which renders an angle of incidence on the sample to be 86°. Gold wire was thermally evaporated onto very clean optical quality glass plate at a pressure of about 10^{-6} Torr. The preparation of such plates were described in detail in the experimental section of chapter 5. Such gold coated glass plates (G) were attached at the wedges. Gold is preferred since it is highly reflecting and does not get oxidized with time. The sample (S) for the RAIRS was prepared by depositing

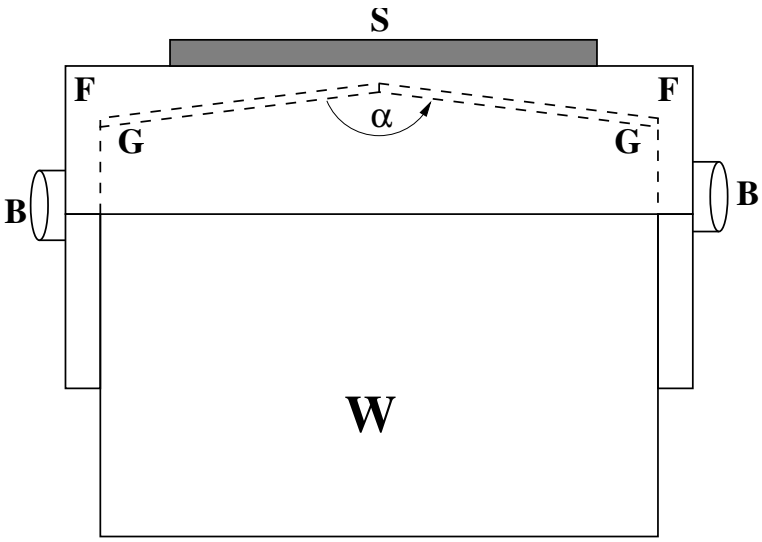

Figure B.1: A schematic diagram of the wedge-setup for the RAIRS. The components are as follows; brass block (W) with a wedge angle α being 176°, sample deposited substrate (S), aluminum frame for holding sample (F), screw for height adjustment of the sample from the wedge (B) and gold coated mirror (G).

LB films on the metallic substrates. An aluminum frame (F) was attached to the brass block to hold the sample. The motion of the frame was restricted only in the Z direction which is normal to the sample plane. Such motion is needed to align the sample so that the outgoing beam is made collinear to that of the incoming beam. This adjustment ensures that the angle of incidence on the sample deposited substrate is 86°.

A complete setup for the study of RAIRS of the thin film is shown in Figure B.2. We

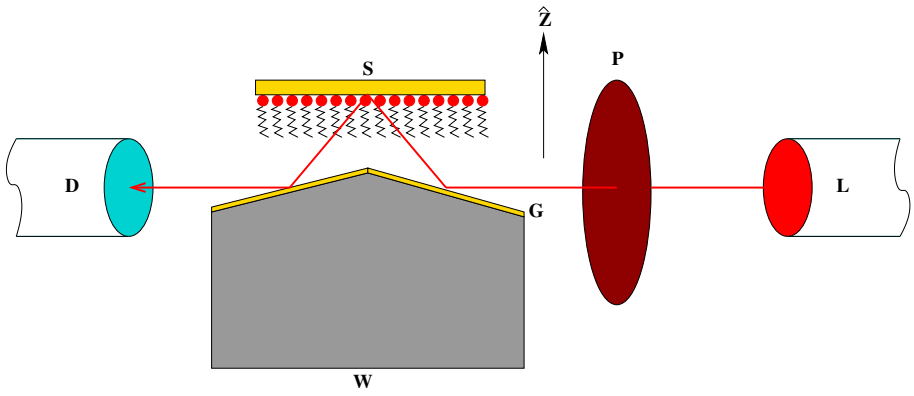

Figure B.2: A schematic diagram of the grazing angle reflection absorption infrared spectroscopy (RAIRS) setup. The components are as follows; IR source (L), IR polarizer (P), brass wedge (W), gold reflectors (G), sample deposited substrate (S) and detector (D).

have used Shimadzu 8400 FTIR spectrometer for the IR experiments. (L) is the IR source

which gives a band of radiation of wavenumber from 400 to 4000 cm^{-1}. The spectrometer was equipped with a sensitive pyroelectric detector (D) with a DLATGS (L-alanine-doped deuterated triglycine sulfate) element. The film deposited substrate (S) was mounted in the RAIRS attachment, as shown in Figure B.2. The radiation from the source (L) gets polarized by an IR polarizer (P) procured from Molectron. The p-polarized light reflected from the gold reflector (G) of the wedge (W) is made to incident on the sample deposited on the substrate (S). The IR beam falls on the sample, then gets reflected from the gold reflector and enters the detector (D). The spectrum was collected by integrating 50 interferrograms. The spectral resolution was 4 cm^{-1}. The background spectra were taken for the bare substrates before the LB films were transferred. The data were collected in ASCII format and were processed using different computer packages. The KBr pellet transmission experiments were performed by making the pellet of known thickness and molar concentration of the compound.

We have employed a home made heater for studying the temperature dependence of the order-disorder transition in the LB films of the stearic acid.

Theory

The spectra from RAIRS of the LB films of the organic molecules show a number of vibrational bands depending upon the functional groups present in the molecule. One particular functional group may give rise to many bands depending upon the types of modes of vibration. For instance, a -CH_2 group can show peaks corresponding to the symmetric and asymmetric stretches, scissoring, rocking, wagging and bending modes at different wavenumbers in the spectrum. The molecular tilt in the LB film can be determined from these bands.

The intensity of absorption (I) (Equation B.1) for a particular mode is proportional to the square of the scalar product of the electric field (E) and the transition dipole moment (M).

$$I = C\,|M.E|^2 \tag{B.1}$$

where C is a constant.

Let us consider a geometry where the transition dipole moment M associated with the molecule makes an angle β with respect to the long molecular axis. The molecular axis makes an angle θ with respect to the substrate normal (Z-axis). The tilt (θ) of the molecule can be determined from the relation

$$cos^2\theta = \frac{2D - 3sin^2\beta}{3\,(3cos^2\beta - 1)} \tag{B.2}$$

where D is defined as

$$D = \frac{I_{LB}}{I_{iso}} = \frac{C|M_zE|^2}{C < |M_zE|^2 >} \tag{B.3}$$

Here, I_{LB} and I_{iso} are the absorbance for the LB film and for the film of isotropically oriented molecules having the same thickness and surface density as that of the LB film, respectively. I_{LB} can be determined from the reflection absorption spectra of the LB films and I_{iso} can be calculated theoretically. To calculate I_{iso}, we have followed the method of D. L. Allara and R. G. Nuzzo (Langmuir **1**, 52 (1985)). I_{LB} and I_{iso} can be used in Equation B.2 to determine the tilt (θ) of the molecules in the LB films.

Experimental

A solution of stearic acid ($C_{17}H_{35}COOH$) having a concentration of 3.5 mM was prepared in HPLC grade chloroform. We have used thermally evaporated aluminum coated glass plates (3.5x3x0.1 cm^3) as the substrates for LB film deposition of stearic acid (SA). The substrate preparation has been discussed in detail in chapter 6. The target surface pressure (π_t) was fixed at 20 mN/m. On attaining the π_t, the monolayer was allowed to equilibrate for about 30 minutes. The dipper speeds for the upward and downward strokes were maintained at 15 mm/min. The LB films were stored in a desiccator for about 30 minutes. The π_t of 20 mN/m corresponds to the liquid condensed ($L'_{2_{SA}}$) phase of the SA on the water surface. In the $L'_{2_{SA}}$ phase, molecules tilt towards its next nearest neighbor on the water surface, and form a distorted hexagonal lattice. All the LB films were prepared at room temperature.

Calibration of the setup with LB films of stearic acid

The reflection absorption FTIR spectra for the LB films of the SA for different layers are shown in Figure B.3. The vibrational modes assignment to the spectral peaks are listed in the Table B.1.

Mode assignment	Observed (cm^{-1})	Reported (cm^{-1})
CH_3 asymmetric stretch ($\nu^{as}_{CH_3}$)	2963	2963
CH_3 symmetric stretch ($\nu^{s}_{CH_3}$)	2880	2876
CH_2 asymmetric stretch ($\nu^{as}_{CH_2}$)	2918	2917
CH_2 symmetric stretch ($\nu^{s}_{CH_2}$)	2849	2849
C=O stretch ($\nu_{C=O}$)	1707	1706
CH_2 scissoring (δ_{CH_2})	1470	1471
CH_2 wagging (ω_{CH_2})	~1150-1380	~1150-1350

Table B.1: Vibrational modes assignment to the different peaks observed in the spectrum. The reported data were obtained from the references [J. Phys. Chem. **94**, 62 (1990)] and [J. Am. Chem. Soc. **112**, 558 (1990)]. The observed values were extracted from the spectrum of LB film of 9 layers.

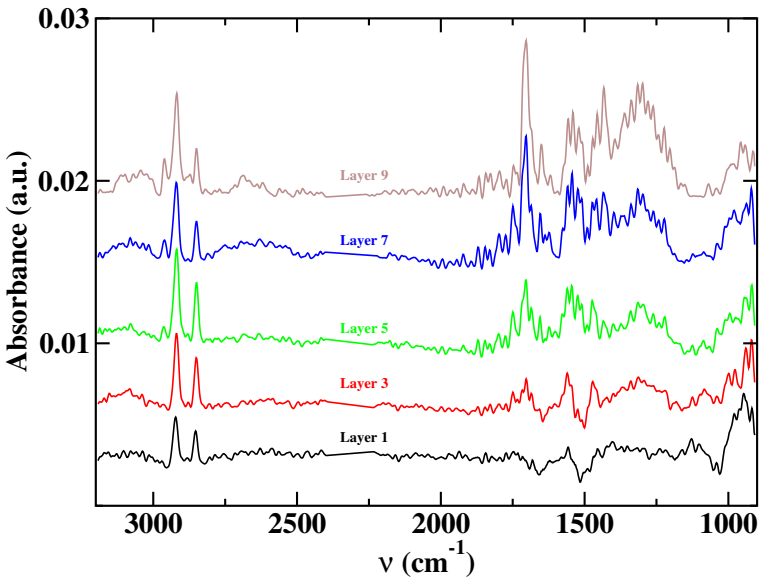

Figure B.3: RAIRS spectra of LB films of stearic acid (SA) for different layers. The spectra are shifted vertically for visual clarity.

The presence of the CH_3 stretching peaks reveals a highly ordered crystallinity in the LB film. The band progression due to the wagging vibration of the CH_2 for one layer is weaker compared to the thicker layers. However, the appearance of very weak peaks could still be observed at the positions specified to the progression bands. The amplitude of the

wagging band is very strong for the layers thicker than 5 layers. The appearance of wagging band suggests a highly ordered crystallinity where the aliphatic chains prefer all trans zigzag configuration.

The area under the peaks (integrated absorbance (I)) were calculated for different characteristic bands. The linear dependence of I on the number of layers for CH_3 asymmetric stretch is shown in Figure B.4. The values of I for other bands also show the linear

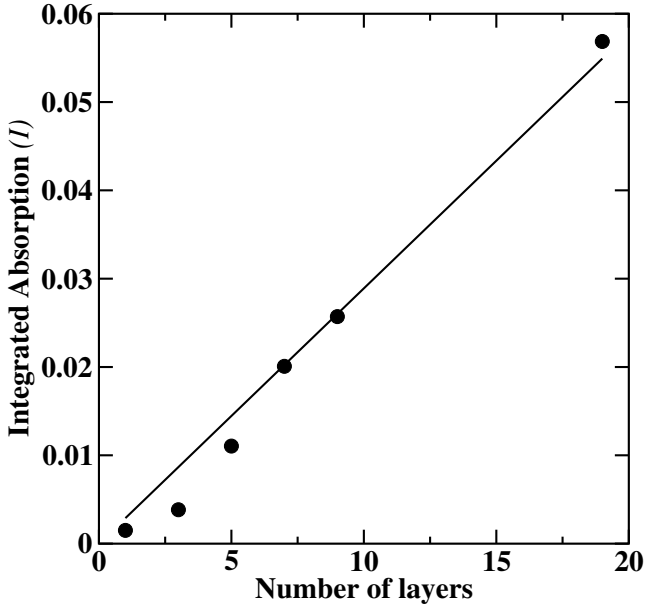

Figure B.4: The variation of integrated absorbance (I) of the CH_3 asymmetric stretch with the number of layers of LB films of stearic acid (SA). The filled circles are the experimentally obtained data, whereas the solid line is the linear fit to the data.

dependence with the number of layers of LB films.

The I_{iso} is calculated theoretically by employing the method given by Allara and Nuzzo (cited above). We performed the experiments on KBr pellets for different concentrations of SA. The spectra are shown in Figure B.5.

The transmission spectra for CH_2 asymmetric band were obtained by computer simulation. We find a good agreement between the experimental and simulated data. This is shown in Figure B.6. We extracted the refractive index (n(ν)) and the extinction coefficient (k(ν)) as a function of wavenumber (ν) from the simulated spectra. These are shown in Figure B.7. The simulated optical parameters thus obtained were utilized in obtaining the I_{iso} for the

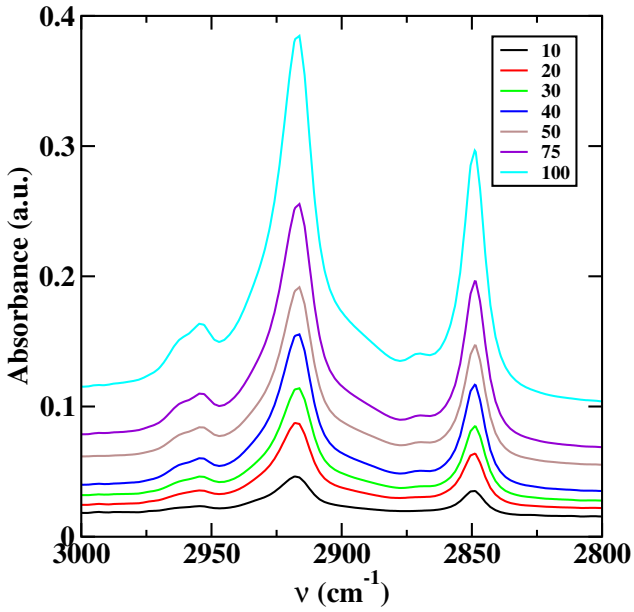

Figure B.5: The spectra for the C-H stretching bands at different concentrations of the stearic acid (SA) molecules in the KBr pellets. The concentration in molecules per cc can be obtained by multiplying 2.083×10^{16} to the number shown in the inset. The spectra are shifted vertically for visual clarity.

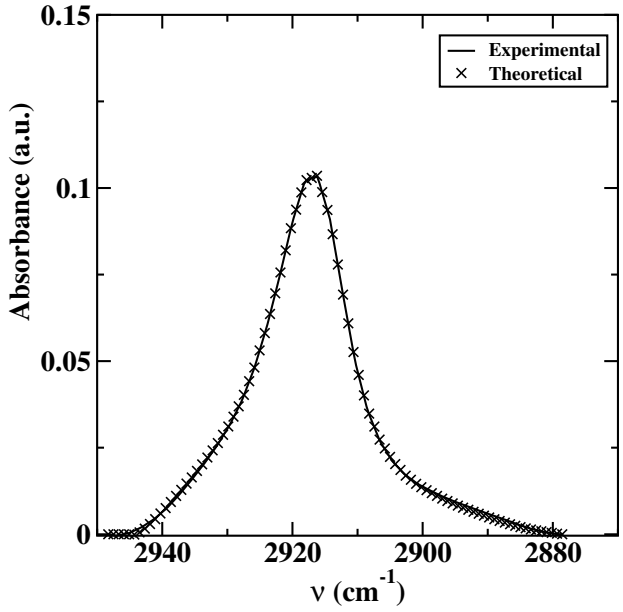

Figure B.6: The experimental and theoretical spectra for CH_2 asymmetric stretching. The concentration of the stearic acid (SA) in the pellet and thickness of the pellet were 8.33×10^{16} molecules per cc and 0.05 cm, respectively. The tolerance for the convergence of the curves was 0.0005.

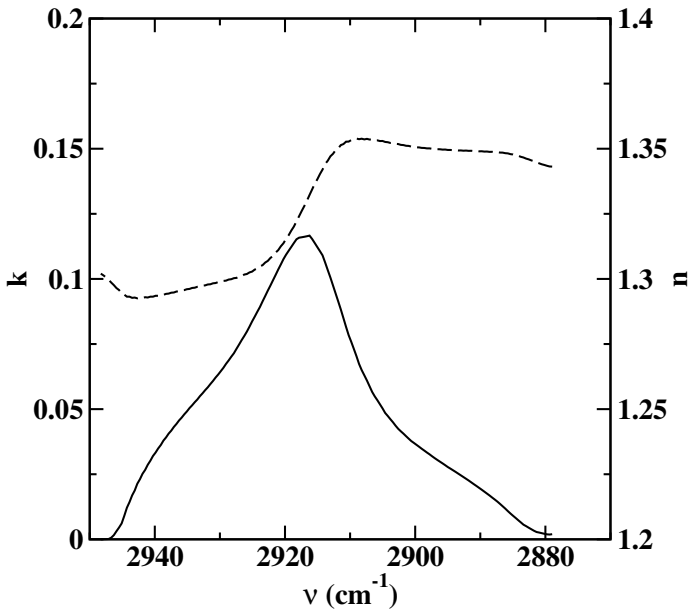

Figure B.7: The refractive index (n(ν)) and extinction coefficient (k(ν)) of the SA (dashed and solid lines, respectively) obtained through computer simulation of the transmission experiment. The concentration of the SA in the pellet was 8.33×10^{16} molecules per cc and the thickness of the pellet was 0.05 cm, respectively.

isotropic film of SA having a monomolecular thickness and of the surface density same as that of one layer of LB film. The simulated reflection absorption spectrum for the CH_2 asymmetric stretch band is shown in Figure B.8. The area under the simulated reflection absorption curve yields the value of I_{iso} which was 1.1738.

The average tilt of the molecules (θ) was calculated using the Equation B.2. It is known that the transition dipole moment (M) corresponding to the asymmetric stretch of the CH_2 makes an angle of 90° with respect to the aliphatic backbone (*i.e.*, C-C-C). We take the value of β equal to 90°. From the reflection absorption spectrum of the one layer of LB film of SA (Figure B.3), we find that the value of I_{LB} is 0.0706. From these, we obtain the value of tilt (θ) of the molecule with respect to the substrate normal to be 11.6°. This is in agreement with the reported value of 12° for the tilt of the SA molecule. Thus, we have shown that we can get reproducible data using a home made RAIRS.

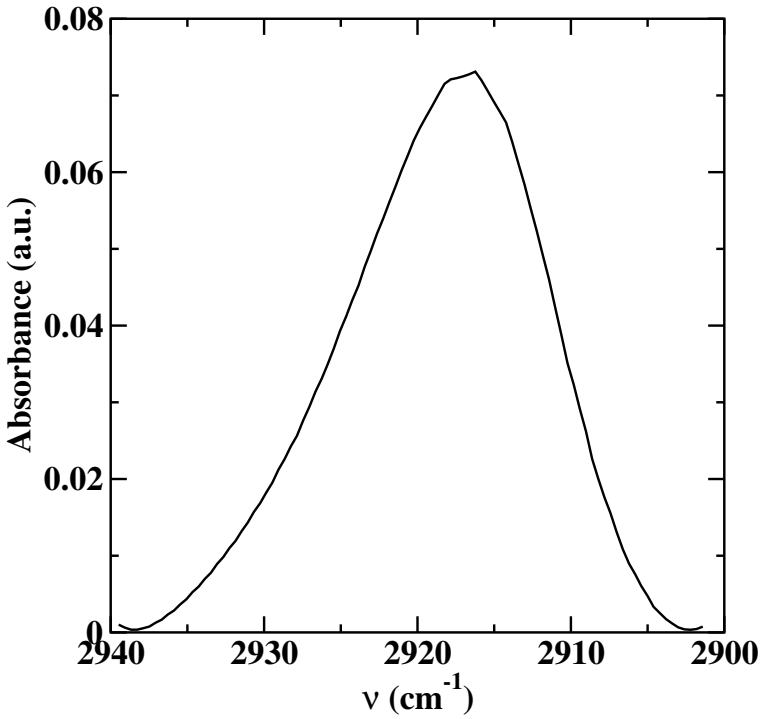

Figure B.8: Simulated reflection absorption spectrum for CH_2 asymmetric stretch of an isotropic film having a monomolecular thickness.

Temperature dependence of the LB films of stearic acid studied using variable-temperature RAIRS

We have employed RAIRS for the study of the thermal behavior of 1, 3, 5, 7, 9, 11, 13, 15, 19 and 29-layers of LB films of SA transferred at a π_t of 30 mN/m on the aluminum substrate. The π_t at 30 mN/m corresponds to the solid phase of SA. In solid phase, the molecules orient normal to the interface on a hexagonal lattice. The spectra for 11-layers of LB film of SA at different temperatures are shown in Figure B.9.

We have analyzed the band corresponding to the C=O stretching. The corresponding transition dipole moment is normal to the molecular axis. For the molecules oriented normal to the substrate, the transition dipole moment is parallel to the substrate. Therefore, the interaction between the transition dipole moment and the p-polarized electric field will be minimum. However, if the molecules are tilted, they will result in increase in the interaction of the incoming beam with the transition dipole moment. This enhances the I values. The values of I for the C=O band at different temperatures were computed for different layers of

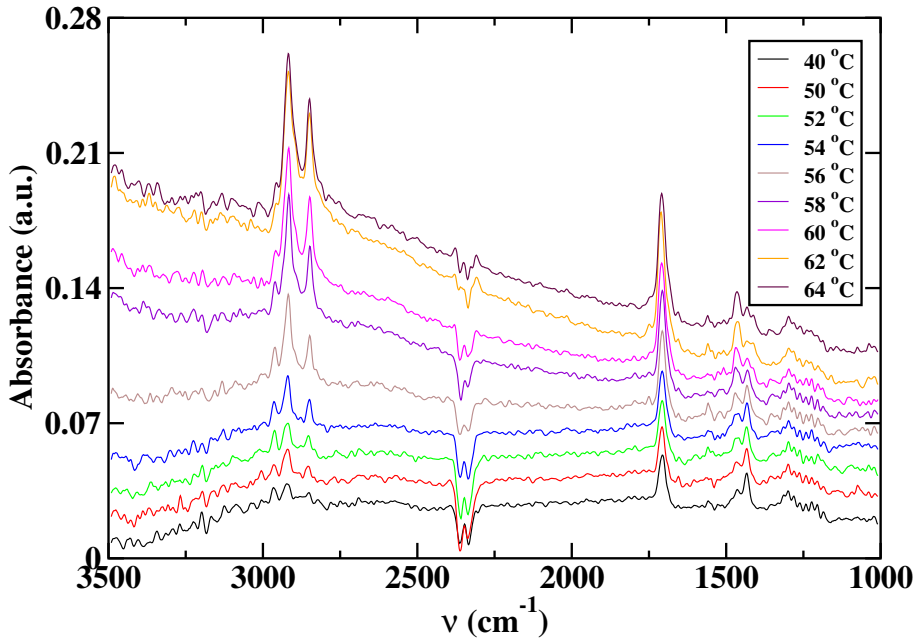

Figure B.9: The RAIRS spectra at different temperatures for 11-layers of LB film of stearic acid (SA) deposited on Al substrate. The spectra are shifted vertically for visual clarity.

LB films of SA (Figure B.10). The variation in *I* with temperature for the three and five layers was very small. The invariant nature of the *I* with temperature for the thinner films like 3 and 5-layers can be due to the strong anchoring of the molecules on the aluminum substrate. The strong anchoring does not allow the molecules to change its states and conformation on the substrate even at a temperature upto 72 °C. However, for more than five layers, the value of *I* remains invariant upto 50 °C. Then the values of *I* started increasing upto 62 °C. Above 62 °C, the values of *I* decrease. Hence, the state of the molecules in the LB films (> 5 layers) was independent of temperature upto 50 °C. Above this temperature, the increase in *I* suggests the increase in average tilt of the molecules. Since the molecules were transferred at 30 mN/m (solid phase), the films were assumed to be homogeneous and free from defects. The increase in *I* values from a temperature range of 50 to 62 °C can be attributed to an increase in average tilt of the molecules. This temperature range can be regarded as a premelting transition region of the LB films of SA. The change in trend of *I* values at 62 °C may indicate the melting of the LB films. Hence, the temperature 62 °C can be regarded as the melting transition temperature of the LB films of SA.

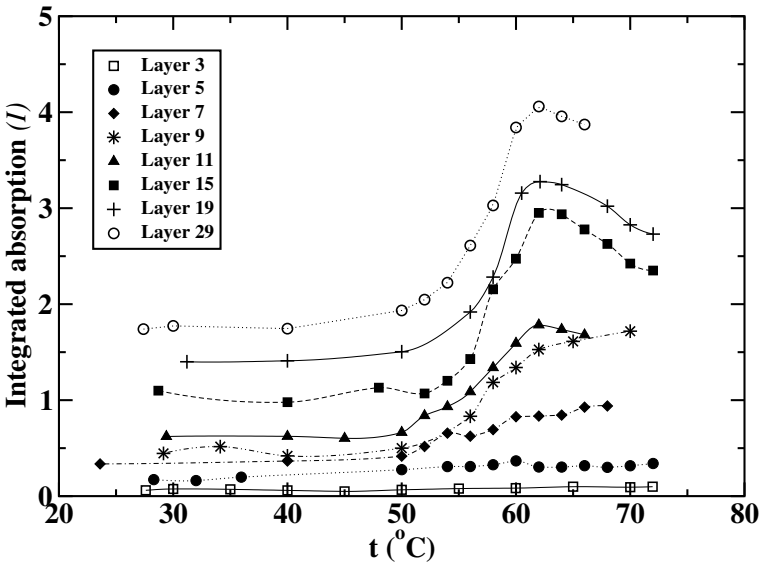

Figure B.10: The variation of integrated absorption corresponding to the C=O bands with temperature obtained during RAIRS experiments on LB films of stearic acid (SA). The lines are guide to the eyes.

We have demonstrated with SA that our home built setup can be used to determine the tilt and ordering of the molecules in the LB films. The characteristic peaks of the SA in the RAIRS spectra were observed even for a single layer of LB film. Hence, the setup can be used to study ultrathin films like a layer of LB film or a self-assembled monolayer.